

Incoherent Quasi-elastic Neutron Scattering from Fructose–Water Solutions

Melissa Feeney,[†] Craig Brown,[‡] Amos Tsai,[‡] Dan Neumann,[‡] and Pablo G. Debenedetti^{*†}

Department of Chemical Engineering, Princeton University, Princeton, New Jersey 08544, and NIST Center for Neutron Research, National Institute of Standards and Technology, Gaithersburg, Maryland 20899

Received: February 14, 2001; In Final Form: June 6, 2001

Quasi-elastic incoherent neutron scattering (QENS) was used to study the dynamics of 4, 29, and 60 wt % solutions of fructose in deionized water at 300 K. Both the jump–diffusion and stretched exponential models were used to analyze the data, enabling the determination of the structural relaxation rate $1/\tau$ and the stretch exponent β as functions of fructose concentration. The analysis of the neutron scattering data based on the jump–diffusion model is consistent with a transition from continuous to “hopping” or jump diffusion at 29 wt % fructose concentration observed in recent simulations of this same system. The analysis based on the stretched exponential model suggests that this change occurs at a higher fructose concentration.

I. Introduction

In the early stages of the development of a protein therapeutic, it is essential to design a formulation that is stable during shipping and long-term storage. Historically this has been achieved through properly prepared lyophilized or freeze-dried formulations, in which carbohydrates make up the majority of the nonactive components.^{1,2} It is thought that carbohydrates protect proteins from both freezing and drying stresses during the lyophilization process.^{3,4} It is also believed that the mechanism responsible for the preservation of proteins during storage and drying are fundamentally different.^{5,6} Protection of the labile proteins during storage appears to be due to the structural arrest and the consequent dramatic slowing down of diffusive processes in the amorphous solid or glassy state. Protection of proteins during dehydration by carbohydrates, on the other hand, is thought to be due to hydrogen bonding between the sugar and the dried protein with the former serving as a water replacement. However, the molecular mechanisms by which particular sugars are able to stabilize and protect labile biomolecules are still not fully understood.⁷ At present, there is no consensus on the detailed roles of specific interactions and of vitrification in the stabilization of dry biomaterials.⁸

With the above points in mind, it is of interest to know how low molecular weight carbohydrate–water solutions evolve toward a glassy state upon dehydration. From the standpoint of the rational design of formulations for preserving labile biologicals, it is desirable to have a molecular-level understanding of how the structure and dynamics of carbohydrate–water solutions are affected by changes in composition. In this work we report incoherent quasi-elastic neutron scattering (QENS) experiments for 4, 29, and 60 wt % solutions of fructose in deionized water at 300 K. The aim of these experiments is to explore the relationship between the dynamics of fructose–water solutions and changes in composition. Since QENS typically measures small energy exchange in the region of ± 2 meV it is frequently used to study the diffusive motion of molecules.⁹ Hydrogen has an unusually large incoherent cross-section,

therefore it dominates the signal of incoherent neutron scattering experiments when it is present in a system. Consequently, incoherent QENS is an effective tool to probe the diffusive motion of molecules containing hydrogen atoms.

Recent related neutron scattering results include studies of the diffusivity of trehalose, a naturally occurring disaccharide of glucose, in aqueous solutions.^{10,11} In the first of these studies, Magazu et al. reported the detection of two distinct translational diffusive mechanisms from QENS experiments.¹⁰ They assigned these mechanisms to the continuous translation diffusion of the trehalose molecules and to the translational jump diffusion of the water molecules. More recently, Magazu et al. used QENS in combination with H/D substitution to distinguish the diffusive dynamics of water from that of trehalose.¹¹ They found that in the presence of trehalose the water translational dynamics suffers a slowing down. In addition to dynamics, neutrons can also provide structural information. Tromp et al. used H/D substitution and wide angle neutron scattering to determine the hydrogen bond structure in glassy and liquid glucose.¹²

Another technique for measuring water mobility in concentrated carbohydrate water solutions is nuclear magnetic resonance (NMR). In a recent ²H NMR study of the glucose–water system, Moran and Jeffery,¹³ used D₂O mixed with ordinary glucose, and deuterated glucose mixed with H₂O. Thus, they were able to measure separately the relaxation times and the diffusion coefficients of water in both the crystalline ice and amorphous glass phases, and of the sugar in the glass phase. The usefulness of NMR in studying concentrated sugar–water systems is not limited to ²H NMR, but also includes ¹H NMR and ¹³C NMR. van den Dries et al. used ¹H NMR to study the molecular mobility of water and carbohydrate protons in maltose samples as a function of water content and temperature.¹⁴ They concluded that water disrupts the stable hydrogen-bond network between sugar molecules, which is formed at the glass transition temperature, by increasing the mobility of hydroxyl protons of maltose. Rampp et al. used a combination of ¹³C NMR and ¹H NMR to study the effect of concentration and temperature on the viscosity and the diffusion coefficients of some disaccharides and fructose.¹⁵ The use of ¹³C NMR, while more time-consuming than ¹H NMR, has the great advantage that it avoids the use of heavy water, thus allowing

* Corresponding author. E-mail: pdebene@princeton.edu.

[†] Princeton University.

[‡] NIST Center for Neutron Research, National Institute of Standards and Technology.

the diffusion coefficient of water to be determined in a much wider range of temperature and concentration.

Finally, we mention molecular simulation, which has emerged in recent years as a powerful method for obtaining microscopic-level information on the structure and dynamics of carbohydrate–water systems.^{7,16,17} Diffusion coefficients, density of states, and scattering functions can be measured directly using both simulations and neutron scattering. Thus, the combined use of these two techniques appears to be a powerful approach to the study of concentrated water–carbohydrate systems. In this work we compare our experimental results with those of recent molecular dynamic simulations.¹⁷

II. Experimental Section

We used the Fermi chopper time-of-flight spectrometer at the Center for Neutron Research at National Institute of Standards and Technology. The neutron beam was monochromated to 6 Å and pulsed at 135 Hz resulting in an energy resolution of $\sim 63 \mu\text{eV}$ for our experiments. Data were collected for momentum transfers $\hbar Q$ ($\hbar = h/2\pi$) corresponding to the range of Q values $0.25 < Q < 2 \text{ \AA}^{-1}$. The typical data collection time was about 24 h.

4, 29, and 60 wt % samples of D-fructose in deionized water were prepared. The sample was placed in an aluminum container with a thin annular radius of 0.1 mm. This radius was chosen to reduce multiple scattering, which complicates data analysis. The container was mounted inside a closed-cycle, He refrigerator. Data were collected at 300 K for the 4, 29, and 60 wt % fructose solutions. A separate empty-cell run was made at 300 K, and the result was subtracted from that of the fructose solutions to remove scattering from the sample cell. Another separate run was made with vanadium in order to obtain the resolution function and the detector efficiency of the spectrometer.

III. Data Processing

The standard way to analyze neutron scattering spectra assumes decoupling between vibrations, rotations, and translational motions.¹⁸ Under this approximation, the scattering function $S(Q, \omega)$ can be expressed as

$$S(Q, \omega) = [S_V(Q, \omega) + S_R(Q, \omega) + S_T(Q, \omega)] \otimes R(\omega) \quad (1)$$

where each term is convoluted with the instrument resolution, $R(\omega)$.¹⁹ $S_V(Q, \omega)$, $S_T(Q, \omega)$, and $S_R(Q, \omega)$ are the vibrational, translational, and rotational scattering functions, Q is the scattering vector, and $\hbar\omega$ is the energy transferred to the sample by a scattered neutron. The time scale of observation of the time-of-flight Fermi chopper spectrometer is approximately 75 ps. This is much longer than the vibrational period of the hydrogen atom. In this long-time limit, the vibrational scattering function is reduced to the Debye–Waller factor.²⁰ Di Cola et al. concluded that for time scales longer than about 1 ps, QENS experiments essentially probe the dynamics of the translational motion, i.e., center of mass dynamics, of water molecules.²¹ This means that for all practical purposes, we simply need a theoretical expression for the translational scattering function in order to analyze high-resolution quasi-elastic neutron scattering (QENS) spectra. To characterize the relaxation, we used two different models to analyze the data.

As mentioned earlier, hydrogen has an unusually large incoherent scattering length, and therefore dominates the scattering function of QENS experiments. It is important to separate the signal from fructose and water in order to study the diffusive

TABLE 1: Percentage of Signal from Water versus Fructose

weight % fructose in solution	% of signal from hydrogen atom in water	% of signal from hydrogen atom in fructose
4	97.6	2.4
29	79.5	20.5
60	52.6	47.4

motion of the water molecules. This was achieved by using a spectrometer whose resolution limit is exceeded by the time scale of the fructose motions.¹⁵ Therefore the sugar scattered elastically and all diffusive motion detected in our system can be attributed to the water molecules. The elastically scattered neutrons from the sugar and the scattering due to the water's diffusive motion compromise the $S_T(Q, \omega)$, which must still be convoluted with the resolution function, a Gaussian, to represent $S(Q, \omega)$. We chose not to use deuterated fructose because fructose contains five exchangeable deuterium atoms. These deuterium atoms would rapidly exchange with the hydrogenated water and therefore we would still need to separate the signal. Table 1 lists the percentage of the total signal due to the hydrogen atoms in fructose versus those in water for each of the solutions studied. The results listed in Table 1 were found by counting the number of hydrogen atoms in water and fructose for each solution. As explained below, the figures reported in Table 1 were used to weigh the appropriate scattering function so as to account for the fraction of the signal due to the water and sugar molecules. In the rest of this section we describe the two different models used to analyze the data and how in each model we accounted for the elastic scattering of the sugar molecules.

(a) Gaussian–Lorentzian Model. The Gaussian–Lorentzian model contains a Gaussian component, which accounts for elastic scattering, and a Lorentzian component, which accounts for all motion detected within a system. Therefore the scattering from sugar molecules is accounted for by a resolution-limited Gaussian component, which is weighted by the fraction of hydrogen atoms in the system that belong to fructose molecules. The scattering of the water molecules is accounted by the Lorentzian component, which is weighted by the percentage of hydrogen atoms in the system that belong to water molecules. These percentages are reported in Table 1.

The translational part of the correlation function results in a sharp Lorentzian peak in the QENS spectrum of the following form:

$$S_T(Q, \omega) \propto \frac{\Gamma(Q)}{[\hbar^2\omega^2 + [\Gamma(Q)]^2]} \quad (2)$$

where $\Gamma(Q)$ is the full width at half-maximum as a function of Q , the scattering vector. The narrowing of $S(Q, \omega)$ at increasing fructose concentration signals the slowing of water motions, and the corresponding line width gives us the characteristic time scale of the motions. This is shown in Figure 1.

The connection between the broadening of the scattering function and diffusion coefficients can be made through Einstein's theory of Brownian motion.²² This continuous diffusion model predicts for $\Gamma(Q)$ the following form

$$\Gamma = 2\hbar D Q^2 \quad (3)$$

where D is the diffusion coefficient. The continuous model breaks down when the strength of intermolecular interactions increases, as in structured liquids. Jump–diffusion models are often used to describe these situations, in which molecules are

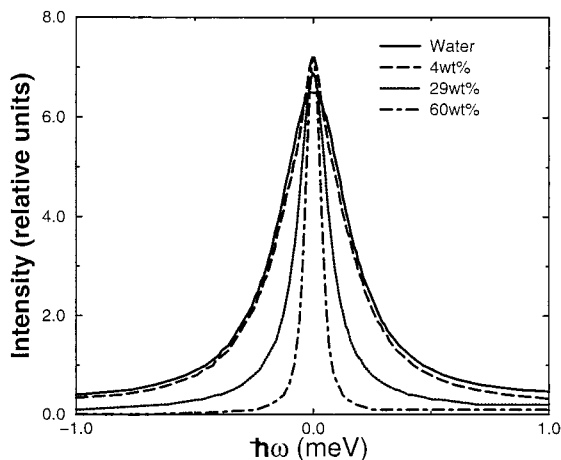


Figure 1. Quasi-elastic incoherent neutron spectra from fructose–water solutions at $Q = 1.0 \text{ \AA}^{-1}$ and $T = 300 \text{ K}$. The narrowing of spectra at increasing fructose concentration signals the slowing of water motions. The quantity plotted is proportional to $S_I(Q, \omega)$ [see eq 2].

assumed to undergo localized oscillatory motions, and occasional translations, during which they diffuse over lengths that exceed the amplitude of localized vibrations.²³ The jump–diffusion model employed here involves the existence of two characteristic times: the jump time τ_j during which the particle diffuses and the residence time τ_o during which it undergoes oscillatory motions without translating.²³ The jump–diffusion model leads to scattering laws in which the quasi-elastic broadening at large Q values deviates noticeably from the DQ^2 law. The full width at half-maximum, Γ , is given in this model by

$$\Gamma = \frac{2\hbar Q^2 D}{1 + Q^2 D \tau_j} \quad (4)$$

The jump time τ_j and the characteristic jump distance l_o are related to the diffusion coefficient by

$$D = \frac{l_o^2}{\tau_j} \quad (5)$$

However, at small Q values, the details of the elementary jump processes are no longer observed and the jump–diffusion law reduces to the continuous model.

(b) Stretched Exponential Model. QENS data can also be analyzed using the Kohlrausch-Williams-Watts (KWW) stretched exponential function,²⁴ which approximates a collection of individual exponential decay processes in a single function with only two parameters, τ and β , in such a way that

$$\exp(-t/\tau)^\beta \approx \sum A_i \exp(-t/\tau_i) \quad (6)$$

Relaxation processes in deeply supercooled liquids are well represented by the KWW function. In low-temperature associating liquids, the center of mass motion can be considered as a compounded motion of a short-time in-cage vibrations and long-time cage relaxation, having two widely separated time scales.²⁵ The cage relaxation at long time can be expressed in terms of the intermediate scattering function as

$$I(Q, t) = A(Q) \exp\left[-\left(\frac{t}{\tau}\right)^\beta\right] \quad (7)$$

In the above eq $1/\tau$ is the relaxation rate; β ($0 \leq \beta \leq 1$) is the

stretch exponent; I , the inverse time Fourier transform of $S(Q, \omega)$, is the intermediate scattering function; and A is the Debye–Waller factor. This equation is routinely applied to model the relaxation behavior in glass-forming microemulsions, polymer melts, polyalcohols, metallic melts, and polyether ketones.^{26–30}

The diffusive motion of the water molecules was modeled by a stretched exponential. The scattering from sugar molecules was accounted for by an elastic component convoluted with the Gaussian resolution. Each component was weighted by the appropriate value given in Table 1. In the stretched-exponential model, the quasi-elastic peak has a line shape that is a Fourier transform of a stretched exponential function. In contrast to the Gaussian–Lorentzian model, the stretched-exponential function has two Q -dependent parameters, $1/\tau$ and β , which characterize the line width. It is convenient to combine the two parameters into a single quantity, the mean relaxation time, $\bar{\tau}$, that characterizes the structural relaxation.²⁰ In the case of an exponential relaxation as a result of continuous diffusion

$$I(Q, t) = \exp(-DQ^2 t) \quad (8)$$

the relaxation can be characterized by its initial slope DQ^2 or by its area $1/DQ^2$. For stretched exponential relaxation, the area under the curve, is utilized to characterize the relaxation process instead of its initial slope, which diverges for $\beta < 1$. For KWW behavior, the area under the curve is given by

$$\bar{\tau} = \int_0^\infty dt \exp\left[-\left(\frac{t}{\tau}\right)^\beta\right] = \frac{\tau}{\beta} \Gamma\left(\frac{1}{\beta}\right) \quad (9)$$

where Γ is the gamma function. The area under the curve is the average relaxation time $\bar{\tau}$. For $Q < 1 \text{ \AA}^{-1}$ a power-law dependence, $\bar{\tau} \propto Q^{-\gamma}$ is observed, with an exponent γ approximately equal to 2. Following Zanotti et al.,²⁰ one can then define an effective diffusion coefficient through the relation

$$\frac{1}{\bar{\tau}} = DQ^2 \quad (10)$$

Note that eq 10 provides an estimate of the average diffusion coefficient.²⁰ It is clearly not an exact relation, because it implies equality between eq 7 and eq 8, which is true only when $\beta = 1$. In other words, when stretched exponential behavior occurs, the average relaxation time has an unambiguous meaning but the diffusion coefficient is only an effective, estimated quantity.²⁰

IV. Results and Discussion

The dynamics of water at different fructose concentrations as represented by the scattering function $S(Q, \omega)$ are presented in Figure 1 at $Q = 1.0 \text{ \AA}^{-1}$. The narrowing of $S(Q, \omega)$ at increasing fructose concentrations signals the slowing of water motions, and the corresponding line width gives us the characteristic time scale of the motions. Similar trends are seen for all experimentally accessible Q values. Both the Gaussian–Lorentzian model and the KWW stretched exponential models were used to estimate the diffusion coefficients of water as a function of fructose concentration. Figure 2 shows the fit of the two models for the 60 wt % fructose solution at a Q value of 1.02 \AA^{-1} . Notice that both are in excellent agreement with the data. Results from the Gaussian–Lorentzian model will be presented first, followed by the results from the stretched-exponential model.

(a) Gaussian–Lorentzian Model. For the Gaussian–Lorentzian model, the slope of Γ versus Q^2 is related to the diffusion

TABLE 2: Comparison of Water Diffusion Coefficients in Fructose (QENS, 2 Models, This Work; MD¹⁷ and NMR¹⁵)

solution	D QENS Gaussian–Lorentzian (10 ⁻⁵ cm ² /s)	D QENS stretched-exponential (10 ⁻⁵ cm ² /s)	D ^a MD simulations ¹⁷ (10 ⁻⁵ cm ² /s)	D ^b NMR ¹⁵ (10 ⁻⁵ cm ² /s)
pure water	2.67 ± 0.05	2.51 ± 0.03	2.58 ± 0.03	
4 wt % fructose	2.51 ± 0.10	2.30 ± 0.06	1.80 ± 0.05	
29 wt % fructose	1.80 ± 0.10	1.50 ± 0.10	0.062 ± 0.005	2.00
50 wt % fructose				0.75
60 wt % fructose	0.71 ± 0.20	0.38 ± 0.08	0.016 ± 0.003	
70 wt % fructose				0.23

^a Roberts, C. J.; Debenedetti, P. G. *J. Phys. Chem. B* **1999**, *103*, 7308. ^b Rampp, M.; Buttersack, C.; Lüdemann, H. D. *Carbohydr. Res.* **2000**, *328*, 561.

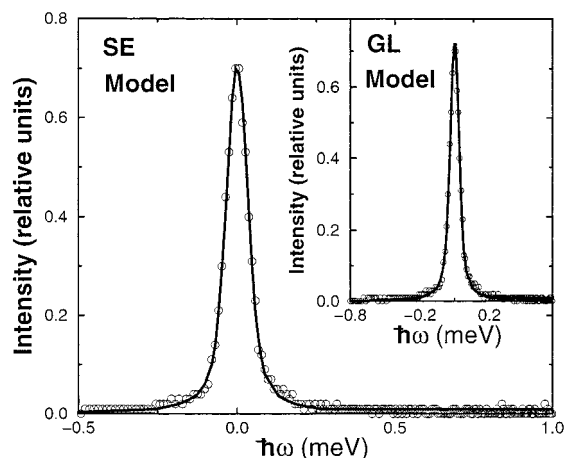


Figure 2. Comparison of the two different methods of analysis of the same QENS data set. The typical spectrum as taken from a 60 wt % fructose–water solution at $Q = 1.0 \text{ \AA}^{-1}$ and $T = 300 \text{ K}$. The empty circles are experimental data; the solid line is the stretched exponential model. In the inset the empty circles are data and the solid line is the Gaussian–Lorentzian model. Notice that both models are in excellent agreement with the data.

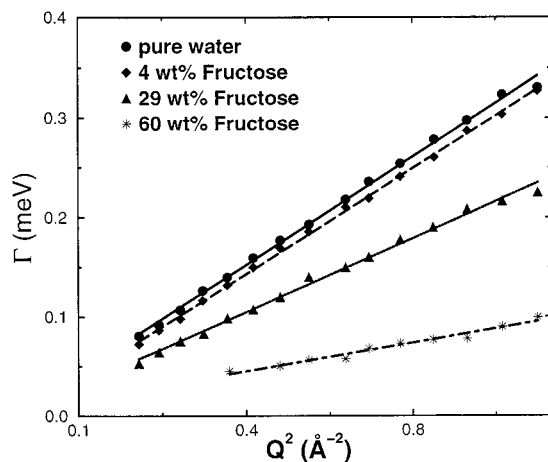


Figure 3. Line width Γ of the translational component of the spectrum versus Q^2 , shown for Q values less than 1 \AA^{-1} . Best fit is given by eq 3, indicating that continuous diffusion dominates at low Q values or large length scales. The decrease of slope for increasing fructose concentrations indicates a slowing of the diffusive motion of water.

coefficient as seen by eq 3 for small Q values, i.e., $Q < 1 \text{ \AA}^{-1}$. Figure 3 shows the linear dependence of Γ versus Q^2 as a function of fructose concentration at Q values less than 1 \AA^{-1} . Values of the diffusion coefficient of pure water, and of water in 4, 29, and 60 wt % solutions are reported in Table 2. These values are based on eq 3 and account for the elastic scattering due to the fructose. They vary from $D^{\text{H}_2\text{O}} = 2.7 \times 10^{-5} \text{ cm}^2/\text{s}$ for pure water to $D^{\text{H}_2\text{O}} = 7.1 \times 10^{-6} \text{ cm}^2/\text{s}$ for water in 60 wt

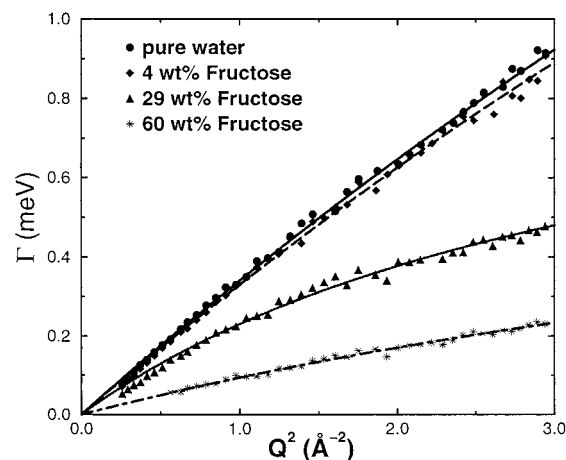


Figure 4. Line width Γ of the translational component of the spectrum versus Q^2 , shown for all Q values. The line width of pure water and the 4 wt % solution varies linearly with Q^2 , suggesting that continuous diffusion dominates, with the best fit given by eq 3. At higher concentrations, the line widths show an initial linear region and then flatten out to a constant value. This confirms the jump–diffusion model for the intermediate-time diffusion of water, with the best fit given by eq 4.

% fructose solution, indicating an order of magnitude drop in the diffusive motion of water upon increasing the fructose concentration. The sensitivity of $D^{\text{H}_2\text{O}}$ to the percentage of the signal attributed to the sugar was tested by systematically increasing (decreasing) the percentage of the signal due to elastic scattering. The error bars included in Table 2 are the direct result of this sensitivity test. We varied the percentage of the signal due to elastic scattering by $\pm 5\%$, which caused the $D^{\text{H}_2\text{O}}$ for the 4 and 29 wt % solutions to differ by 4–10% from the results in Table 2. However, for the more concentrated solution, 60 wt % fructose, the same changes in the amount of elastic scattering caused $D^{\text{H}_2\text{O}}$ to vary by as much as 30% from the results reported in Table 2. The increased sensitivity to the elastic component for the 60 wt % data is likely due to the poor statistics at low Q values.

Figure 4 shows Γ versus Q^2 as a function of fructose concentration for all Q values measured. For pure water and the 4 wt % solution the line widths vary linearly with Q^2 and therefore can be described by the continuous diffusion model. The dynamics of these solutions are not controlled by highly cooperative molecular rearrangements. However, at higher fructose concentrations, the line widths show an initial linear region but then start to flatten toward a constant value given by $2/\tau_j$, eq 4. This is a striking confirmation of the jump–diffusion model for the intermediate time diffusion of water. This is consistent with the suggestion that in concentrated carbohydrate solutions, water molecules diffuse by “hopping” over preferential jump distances, l_0 . The transition in diffusion

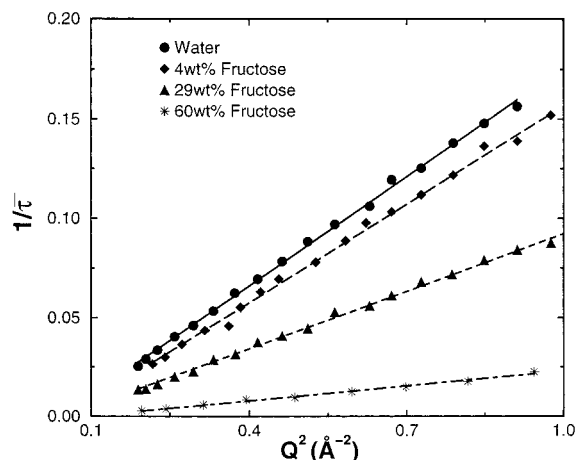


Figure 5. The inverse of the average relaxation time $\bar{\tau}$ [defined by eq 9] for pure water and 4, 29, and 60 wt % fructose solutions versus Q^2 . The slope decreases for increasing fructose concentration, signaling the progressive slowing of water's translation motion.

from continuous, hydrodynamic behavior to “hopping” is observed at 300 K, well above the glass transition temperature (T_g) for the 29 wt % or 60 wt % fructose solutions, which are 149 K and 190 K, respectively.³¹ The occurrence of “hopping” is expected in more concentrated carbohydrate water solutions because the macroscopic translational mobility becomes more strongly influenced by the need for highly cooperative molecular rearrangements.

(b) KKW Stretched-Exponential Model. The slope of $1/\bar{\tau}$ versus Q^2 is related to the average diffusion coefficient as seen by eq 10 for small Q values. Figure 5 is a plot of $1/\bar{\tau}$ versus Q^2 as a function of fructose concentrations for Q values less than 1 \AA^{-1} . Based on eq 10 the values for D are calculated and listed in Table 2. Like the values calculated based on eq 3, these values of $D^{\text{H}_2\text{O}}$ also account for the elastic or Gaussian signal due to the fructose. These values vary from $D^{\text{H}_2\text{O}} = 2.5 \times 10^{-5} \text{ cm}^2/\text{s}$ for pure water to $D^{\text{H}_2\text{O}} = 3.8 \times 10^{-6} \text{ cm}^2/\text{s}$ for water in 60 wt % fructose solution. Again, to obtain error estimates, the sensitivity of $D^{\text{H}_2\text{O}}$ to the percentage of the signal attributed to the sugar was tested by systematically increasing (decreasing) the percentage of the signal due to elastic scattering. We varied the elastic scattering by $\pm 5\%$ from the values given in Table 1, causing $D^{\text{H}_2\text{O}}$ for the 4 and 29 wt % solutions to differ by 2–8% from the results reported in Table 2. However, for the more concentrated solution, 60 wt % fructose, the same changes in the amount of elastic scattering caused $D^{\text{H}_2\text{O}}$ to vary by as much as 20% from the results reported in Table 2. Again, the larger changes at the high concentration are likely due to the poor statistics of the 60 wt % data at low Q values. The values of $D^{\text{H}_2\text{O}}$ obtained by using the Gaussian–Lorentzian model and the stretched-exponential model differ by 6% for pure water and by as much as 46% for the 60 wt % fructose solution. For pure water, this difference is due to the fact that eq 10 is not exact. With increasing fructose concentration, not only are the differences between measured (jump diffusion) and effective (stretched exponential) diffusivities more pronounced, but poorer statistics (smaller fraction of the signal due to water, see Table 1) may also contribute to this difference.

In addition to the diffusivity values obtained in this work, Table 2 also lists values for $D^{\text{H}_2\text{O}}$ calculated by molecular dynamics (MD) simulations of fructose–water solutions,¹⁷ and recent NMR data¹⁵ for this same system. Aqueous D-fructose contains various tautomeric forms. At 303 K these include 2% α -pyranose, 70% β -pyranose, 5% α -furanose, and 23% β -fur-

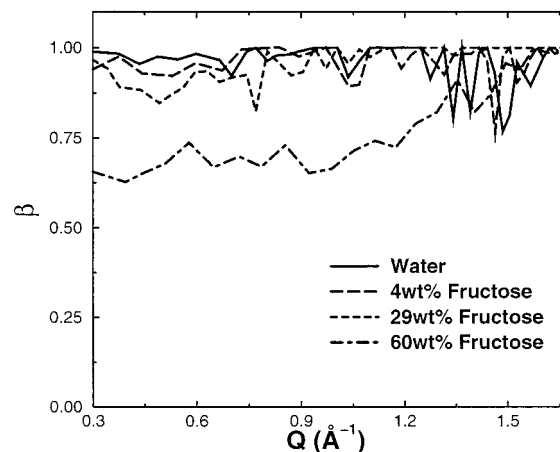


Figure 6. Results from the fitting procedure for the parameter β of the stretched exponential model. β is plotted as a function of both fructose concentration and Q . Note the decrease in β with increasing fructose concentration.

nanose.³² While inorganic compounds and temperature affect the equilibrium distribution of anomers in solution, sugar concentration appears not to affect anomeric equilibrium.³² Only the most stable form, β -pyranose was used in the MD simulations, as accounting for the transformation between the various anomers is beyond the range of what is currently possible in MD simulations. The values of $D^{\text{H}_2\text{O}}$ predicted by the MD simulations decrease by more than 2 orders of magnitude in going from pure water to the 60 wt % solution. Both recent NMR data and our QENS data show that $D^{\text{H}_2\text{O}}$ decreases less sharply as a function of increasing sugar concentration. This is probably due to the fact that the force fields used in the simulations were developed for dilute sugar solutions. This hypothesis is consistent with the agreement seen in Table 2 for pure water diffusivities and for $D^{\text{H}_2\text{O}}$ in 4% fructose, for which the MD results are within 25% of the experimental values. It is important to note that while the force fields do not accurately predict diffusion coefficients for the concentrated solutions, they are still capable of capturing the different mechanisms of diffusion, such as the transition from continuous to jump diffusion occurring around 29 wt % sugar concentration.¹⁷

The dependence of the stretch exponent β on fructose concentration and on Q is shown in Figure 6. It can be seen that there is an insignificant deviation of β from 1 for water, and 4 wt % fructose, and deviations are quite small also for the 29 wt % fructose solution. β is appreciably smaller than 1 for the 60 wt % fructose solution ($Q < 1.4 \text{ \AA}^{-1}$), increasing from ~ 0.63 ($Q = 0.3 \text{ \AA}^{-1}$) to ~ 0.88 ($Q = 1.4 \text{ \AA}^{-1}$). This suggests that a change in the mechanism of water diffusion occurs between 29% and 60 wt % fructose concentration. The analysis based on the Gaussian–Lorentzian model (Figure 4) and previous MD simulations¹⁷ suggest that the transition occurs at 29 wt % fructose. Using the Gaussian–Lorentzian model a plot of Γ vs Q^2 yielded a straight line indicating continuous diffusion for $Q < 1 \text{ \AA}^{-1}$, for all solutions. However, the significant deviation in β from 1 at values of $Q < 1 \text{ \AA}^{-1}$ for the 60 wt % fructose solution suggests that “hopping” entails cooperative events occurring over appreciable length scales. The same progression in relaxation behavior with respect to carbohydrate concentration can be seen in Figure 7. Finally, returning to Figure 6, we note that beyond $Q = 1.5 \text{ \AA}^{-1}$, β appears to be less sensitive to fructose concentration. This suggests that the effect of fructose on water dynamics is felt at length scales greater than 7 \AA . Such a length scale is relevant to the breakage and formation of water cages, rather than the short-time

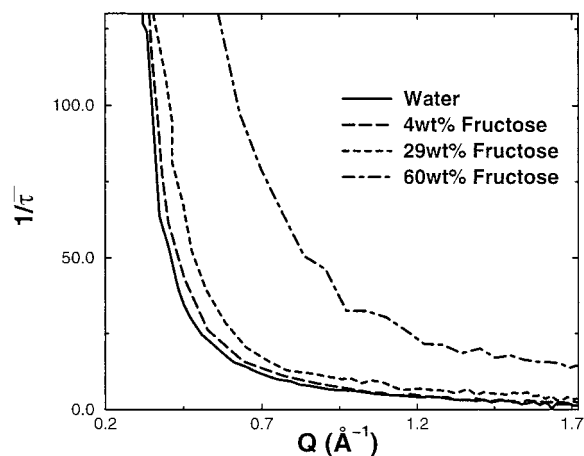


Figure 7. Results from the fitting procedure for the parameter $\bar{\tau}$ of the stretched exponential model. $\bar{\tau}^{-1}$ is plotted as a function of both fructose concentration and Q . Note the decrease in $\bar{\tau}^{-1}$ with increasing fructose concentration.

vibrations of water molecules within the cages. The results suggest that fructose affects the long-time dynamics of water motion, not the short-time vibrations within a cage.

Recently, a correspondence has been found between changes in dynamic behavior and the manner in which glass-forming liquids sample their energy landscape upon cooling.³³ Specifically, it was found that the onset of stretched exponential dynamics and super-Arrhenius activation energies occur at a threshold temperature, below which the depth of potential energy minima sampled by the liquid increases, and above which they remain constant. This threshold temperature therefore marks the onset of a “landscape-influenced” regime, where the dearth of kinetic energy forces the liquid to sample the deeper basins of its energy landscape. Seen in this light, the results of Figures 6 and 7 suggest that increased fructose concentration roughens the mixture’s energy landscape. Sampling this increasingly complex topography results in progressively nonexponential investigation of the water–fructose energy landscape as a function of fructose concentration. It is important to note, however, that the type of calculation on which this reasoning is based has so far only been done for simple mixtures of atomic liquids³³ and for pure water.³⁴

V. Conclusions

Using quasi-elastic neutron scattering, binary solutions of water and fructose have been studied from the dilute to concentrated regimes. To gain insight into both the characteristic type of diffusion and the relaxation properties of the system, both the Gaussian–Lorentzian and the KKW stretched-exponential models were used to analyze the data. Diffusion coefficients were calculated using both models for pure water, 4, 29, and 60 wt % fructose solutions. The analysis of the neutron scattering data based on the Gaussian–Lorentzian model is consistent with the transition from a continuous to a “hopping” or activated diffusion at 29 wt % fructose, as observed in recent MD simulations.¹⁷ The analysis based on the KKW stretched-exponential model suggests that this transition occurs at higher concentrations lying between 29 and 60 wt %. The results from the fitting procedure for the values of the parameter β of the stretched-exponential model were in agreement with fructose affecting the cage relaxation or long-time dynamics of water. On the basis of these findings, we are hopeful that future work will shed more light on the structure and dynamics of sugar water solutions including the glassy state, giving insight into

how proteins are stabilized under these conditions. This insight may be found more directly by studying the nature of cryoprotective ability of sugars in multicomponent systems.

Acknowledgment. P.G.D. gratefully acknowledges the support of the U.S. Department of Energy, Office of Basic Energy Sciences, through Grant DE-FG02-87ER13714. M.R.F. acknowledges the National Science Foundation for a Graduate Fellowship.

References and Notes

- (1) Franks, F.; Hatley, R. H. M.; Mathias, S. F. *Biopharm.* **1991**, *4*, 38.
- (2) Franks, F.; Grigera, J. R. *Water Science Reviews* **5**; Franks, F., Ed.; Cambridge University Press: Cambridge, U.K., 1990; Chapter 4 and references therein.
- (3) Carpenter, J. F.; Prestrelski, S. J.; Arakawa, T. *Arch. Biochem. Biophys.* **1993**, *303*, 456.
- (4) Crowe, J. H.; Crowe, L. M.; Carpenter, J. F.; Rudolph, A. S.; Awistrom, C. A.; Spargo, B. J.; Anchordoguy, T. J. *Biochim. Biophys. Acta* **1988**, *947*, 367.
- (5) Angell, C. A. *Science* **1995**, *267*, 1924.
- (6) Carpenter, J. F.; Prestrelski, S. J.; Anchordoguy, T. J.; Arakawa, R. *Formulation and Delivery of Proteins and Peptides*; ACS Symposium Series 567; American Chemical Society: Washington, DC, 1994; Chapter 9.
- (7) Conrad, P. B.; de Pablo, J. J. *J. Phys. Chem. A* **1999**, *103*, 4049.
- (8) Crowe, J. H.; Carpenter, J. F.; Crowe, L. M. *Annu. Rev. Physiol.* **1998**, *60*, 73.
- (9) Bee, M. *Quasielastic Neutron Scattering*; Adam Hilger: Bristol, U.K., 1998.
- (10) Magazu, S.; Maisano, G.; Majolino, D. *Prog. Theor. Phys. Suppl.* **1997**, *126*, 195.
- (11) Magazu, S.; Lechner, R. E.; Longeville, S.; Maisano, G.; Majolino, D.; Migliardo, P.; Wanderlingh, U. *Physica B* **2000**, *276*, 475.
- (12) Tromp, R. H.; Parker, R.; Ring, S. G. *J. Chem. Phys.* **1997**, *107*, 6038.
- (13) Moran, G. R.; Jeffrey, K. R. *J. Chem. Phys.* **1999**, *110*, 3471.
- (14) van den Dries, I. J.; van Dusschoten, D.; Hemminga, M. A. *J. Phys. Chem. B* **1998**, *102*, 10483.
- (15) Rapp, M.; Buttersack, C.; Lüdemann, H. D. *Carbohydr. Res.* **2000**, *328*, 561.
- (16) Ekdawi, N. C.; Conrad, P. B.; de Pablo, J. J. *J. Phys. Chem. A* **2001**, *105*, 734.
- (17) Roberts, C. J.; Debenedetti, P. G. *J. Phys. Chem. B* **1999**, *103*, 7308.
- (18) Chen, S. H. *Hydrogen-Bonded Liquids*; Vol. 329 of NATO Advanced Study Institute Series C: Mathematical and Physical Sciences; Dore, J. C., Teixeira, J., Eds.; Kluwer Academic Publishers: Dordrecht, N.L., 1991; p 289.
- (19) Teixeira, J.; Bellissent-Funel, M. C.; Chen, S. H.; Dianoux, A. J. *Phys. Rev. A* **1985**, *31*, 1913.
- (20) Zanotti, J. M.; Bellissent-Funel, M. C.; Chen, S. H. *Phys. Rev. E* **1999**, *59*, 3084.
- (21) Di Cola, D.; Deriu, A.; Sampoli, M.; Torcini, A. *J. Chem. Phys.* **1996**, *104*, 4223.
- (22) Einstein, A. *Ann. Phys. Leipzig* **1905**, *17*, 549.
- (23) Chudley, G. T.; Elliott, R. J. *Proc. Phys. Soc.* **1961**, *77*, 353.
- (24) Fuchs, M. J. *Non-Cryst. Solids* **1994**, *172*, 241.
- (25) Sciortino, F.; Gallo, P.; Tartaglia, P.; Chen, S. H. *Phys. Rev. E* **1996**, *54*, 6331.
- (26) Sheu, E. Y.; Chen, S. H.; Huang, J. S.; Sung, J. C. *Phys. Rev. E* **1989**, *39*, 5867.
- (27) Bello, A.; Laredo, E.; Grimau, M.; Nogales, A.; Ezqueria, T. A. *J. Chem. Phys.* **2000**, *113*, 863.
- (28) Weiss, M.; Moske, M.; Samwer, K. *Phys. Rev. B* **1998**, *58*, 9062.
- (29) Paluch, M.; Patkowski, A.; Fischer, E. W. *Phys. Rev. Lett.* **2000**, *85*, 2140.
- (30) Colmenero, J.; Alegria, A.; Arbe, A.; Frick, B. *Phys. Rev. Lett.* **1992**, *69*, 478.
- (31) Ablett, S.; Izzard, M. J.; Lillford, P. J.; Arvanitoyannis, I.; Blanchard, J. M. V. *Carbohydr. Res.* **1993**, *246*, 13.
- (32) Angyal, S. J. In *Advances in Carbohydrate Chemistry and Biochemistry*; Tipson, R. S., Horton, D., Eds.; Academic: New York, 1984; Vol. 42, pp 15–68.
- (33) Sastry, S.; Debenedetti, P. G.; Stillinger, F. *Nature* **1998**, *393*, 554.
- (34) Scala, A.; Starr, F.; La Nave, E.; Sciortino, F.; Stanley, H. E. *Nature* **2000**, *406*, 166.